8. H. Skogby, D. R. Bell, G. R. Rossman, *Am. Mineral.* **75**, 764 (1990).
9. T. E. Young, H. W. Green, A. M. Hofmeister, D. Walker, *Phys. Chem. Miner.* **19**, 409 (1993).
10. A number of high-pressure hydrous silicate phases have been identified. In general, their compositions (for example, their Mg/Si ratio) are not compatible with bulk mantle chemistry [L. W. Finger and C. T. Prewitt, *Geophys. Res. Lett.* **16**, 1395 (1989)].
11. J. E. Dixon, E. M. Stolper, J. R. Delaney, *Earth Planet. Sci. Lett.* **90**, 87 (1988).
12. Spectroscopic studies of defect hydrogen require single-crystal samples to distinguish between hydrogen bound in the crystal structure and that adsorbed on grain boundaries. The intensity of the hydroxyl absorption peaks from these crystals is several orders of magnitude lower than the mid-infrared normal modes that have been documented for (Mg,Fe)SiO_3 perovskite [Q. Williams, R. Jeanloz, P. McMillan, *J. Geophys. Res.* **92**, 8116 (1987)].
13. M. Hanfland, R. J. Hemley, H. K. Mao, G. P. Williams, *Phys. Rev. Lett.* **69**, 1129 (1992).
14. E. Ito and D. J. Weidner, *Geophys. Res. Lett.* **13**, 464 (1986). The end member composition used in this study is the most amenable for the growth of large single crystals.
15. R. J. Hemley and R. E. Cohen, *Annu. Rev. Earth Planet. Sci.* **20**, 553 (1992). Similar single crystals of silicate perovskite have been extensively documented through x-ray diffraction studies [H. Horiuchi, E. Ito, D. Weidner, *Am. Mineral.* **72**, 357 (1987); Y. Kudoh, C. T. Prewitt, L. W. Finger, A. Daravskikh, E. Ito, *Geophys. Res. Lett.* **17**, 1481 (1990)].
16. Microprobe analysis for a single crystal from the same synthesis run has been published [Y. Kudoh, E. Ito, H. Takeda, *Phys. Chem. Miner.* **14**, 350 (1987)]. The most abundant impurities (by weight) are Al_2O_3 (0.33%), P_2O_5 (0.15%), and V_2O_3 (0.12%).
17. The laboratory measurements were carried out at the Smithsonian Institution with a Spectra-Tech IR Plan microscope coupled to a Mattson Cygnus interferometer with a liquid nitrogen–cooled MCT detector. The measurements were made with 2 and 4 cm^{-1} resolution. These and the synchrotron measurements were performed on unoriented single crystals mounted in a nitrogen-purged atmosphere on diamond or BaF_2 substrates. The background spectra were collected from regions adjacent to the crystal.
18. In these samples, the bending mode of the H_2O molecule is observed at 1634 cm^{-1}.
19. G. P. Williams, *Rev. Sci. Instrum.* **63**, 1535 (1992).
20. The synchrotron measurements were carried out with a Spectra Tech IRμs microscope and interferometer with a resolution of 4 cm^{-1}. For many materials, the spatial resolution of this system is limited only by the wavelength of the absorption measurement (*13*). Because of the strong characteristic polarization of synchrotron radiation, the unpolarized measurements from this microscope are actually ~50% polarized.
21. Accounting for differences in the crystal sizes, the signal-to-noise ratio of our laboratory measurements is comparable to that of recent spectroscopic studies of defect hydrogen in samples of SiO_2 stishovite that were synthesized at high pressures (*7*). Notably, the infrared absorbance of the hydroxyl peaks in perovskite is 0.5 to 0.1 of that in stishovite.
22. The Beer-Lambert law can be expressed as $A = \epsilon cl$, where A is integrated absorbance, c is the molar concentration of hydrogen, l is the path length through the sample, and ϵ is the molar absorption coefficient for hydrogen.
23. M. Paterson, *Bull. Mineral.* **105**, 20 (1982).
24. The error in this estimate is predominantly influenced by the uncertainty in the molar absorption coefficient for hydrogen (ϵ) (*4*). For this purpose, we have used a value of 40,000 ± 10,000 cm^{-2} per mole of H per liter (*23*). By comparison, direct ion probe measurements of deuterium contents in samples of this size and concentration are typically uncertain to ±50% (*7*).
25. A. Novak, *Struct. Bonding* **18**, 177 (1974).
26. By comparison, spectroscopic (*7*) and neutron diffraction studies [R. J. Swope and J. Smyth, *Eos* **73**, 651 (1992)] suggest that hydrogen bonding in stishovite occurs along one of the SiO_6 octahedral edges.
27. A. Wall and G. D. Price, in *Perovskite*, A. Navrotsky and D. J. Weidner, Eds. (American Geophysical Union, Washington, DC, 1989), pp. 45–53; D. M. Smyth, *ibid.*, pp. 99–103.
28. Comparisons between equation-of-state measurements on hydrous minerals and seismic density models suggest that the lower mantle could contain up to 2% H_2O by weight [T. S. Duffy, T. J. Ahrens, M. A. Lange, *J. Geophys. Res.* **96**, 14319 (1991); J. A. Tyburczy, T. S. Duffy, T. J. Ahrens, M. A. Lange, *ibid.*, p. 18011].

29. We thank M. Baker for help with the laboratory infrared measurements, and G. Williams, R. J. Hemley, and L. Carr for providing beam time to set up an infrared microscope at the National Synchrotron Light Source. We are grateful to D. Bell, R. Cohen, T. Duffy, L. Finger, R. Hazen, R. J. Hemley, R. Jeanloz, and C. T. Prewitt for discussions and comments. Supported by the NSF Center for High Pressure Research.

23 February 1994; accepted 2 May 1994

Force Detection of Nuclear Magnetic Resonance

D. Rugar,* O. Züger, S. Hoen, C. S. Yannoni,* H.-M. Vieth,†
R. D. Kendrick

Micromechanical sensing of magnetic force was used to detect nuclear magnetic resonance with exceptional sensitivity and spatial resolution. With a 900 angstrom thick silicon nitride cantilever capable of detecting subfemtonewton forces, a single shot sensitivity of 1.6×10^{13} protons was achieved for an ammonium nitrate sample mounted on the cantilever. A nearby millimeter-size iron particle produced a 600 tesla per meter magnetic field gradient, resulting in a spatial resolution of 2.6 micrometers in one dimension. These results suggest that magnetic force sensing is a viable approach for enhancing the sensitivity and spatial resolution of nuclear magnetic resonance microimaging.

It was recently proposed by Sidles and co-workers (*1–3*) that nuclear magnetic resonance imaging with single spin sensitivity and atomic resolution might be achievable with ultrasensitive force detection techniques. In one possible implementation, a microfabricated cantilever operating at low temperature would detect the weak magnetic force acting between a small ferromagnetic particle and the precessing nuclear spins in the sample. The envisioned "magnetic resonance force microscope" would have elemental identification capability and be able to determine nuclear positions with subangstrom spatial resolution in three dimensions. Such an instrument, if it could be built, would represent a revolutionary advance for the field of magnetic resonance imaging and would greatly facilitate the determination of molecular structures.

The first experiments demonstrating the basic principles of magnetic resonance force microscopy were reported recently. Rugar *et al.* (*4*) detected electron spin resonance (ESR) by using an atomic force microscope cantilever to measure an oscillatory 10^{-14}-N magnetic force acting on a 30-ng sample of diphenylpicrylhydrazyl (DPPH). Subsequent imaging experiments by Züger and Rugar (*5*) showed that spatial maps of the magnetic force could be used to reconstruct the electron spin density of the sample with micrometer spatial resolution.

Here, we report the use of micromechanical force sensing techniques to detect nuclear magnetic resonance (NMR). Compared to the previous ESR work, NMR force detection is considerably more challenging because the magnetic moments of common nuclei are at least 650 times smaller than the moment of the electron. Furthermore, nuclei have much longer spin-lattice relaxation times, necessitating a different approach for manipulating the spin magnetization. We have overcome these obstacles by (i) fabricating ultrathin cantilevers that improve our force detection sensitivity to 5×10^{-16} N; (ii) operating the force detection apparatus in a high magnetic field (2.35 T) to enhance the nuclear polarization; and (iii) implementing a magnetization modulation technique based on cyclic adiabatic inversion (*6*). These innovations, in combination with the 600-T/m field gradient generated by a millimeter-size iron particle, resulted in a single shot NMR sensitivity of 1.6×10^{13} protons and a spatial resolution of 2.6 μm.

The force detection apparatus (Fig. 1) fit within the room-temperature bore of a superconducting magnet and was operated in a $<10^{-3}$-torr vacuum to avoid air damping of the cantilever. The sample consisted of 12 ng of ammonium nitrate, which was glued onto a custom-fabricated silicon ni-

---

IBM Research Division, Almaden Research Center, 650 Harry Road, San Jose, CA 95120, USA.

*To whom correspondence should be addressed.
†Present address: Institut für Experimentalphysik, Freie Universität Berlin, D-14195 Berlin, Germany.

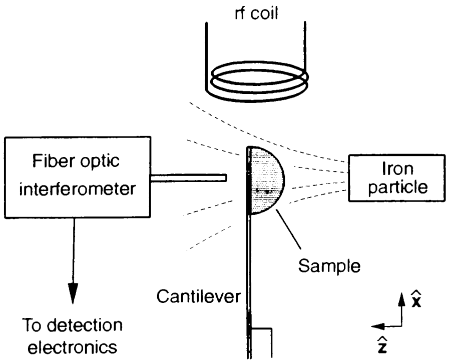

Fig. 1. Basic configuration of the force detection apparatus. Protons in the sample are polarized by the combination of a homogeneous field from a superconducting magnet (not shown) and the inhomogeneous field (dashed lines) from a magnetized iron particle. The *z* component of sample magnetization is made to oscillate by means of the cyclic adiabatic inversion induced by frequency modulation of an applied rf field. The oscillating magnetization in the presence of the inhomogeneous field generates an oscillating magnetic force and causes the cantilever to vibrate. The vibration amplitude is measured with the use of a fiber optic interferometer and a lock-in amplifier.

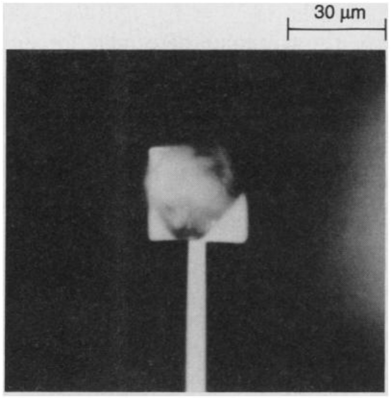

Fig. 2. Optical micrograph of the 900 Å thick silicon nitride cantilever. A small grain of the sample material (ammonium nitrate) is visible on the upper portion of the paddle-shaped cantilever. The narrow neck of the cantilever is 50 μm long and 5 μm wide.

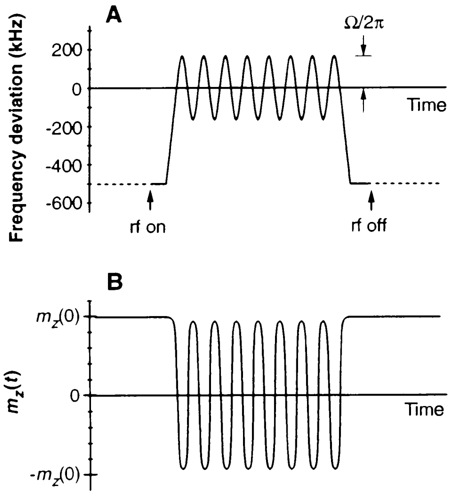

Fig. 3. (**A**) Frequency modulation pattern used for cyclic adiabatic inversion. The plotted quantity is the rf frequency deviation $\Delta\omega(t)/2\pi$. In the actual experiment, the modulation typically persists for several thousand cycles. (**B**) The resulting *z* component of magnetic moment calculated by assuming that the nuclear magnetization follows the direction of the effective field (Eq. 2).

tride cantilever (*7*). Ammonium nitrate was chosen as the sample material because of its abundance of hydrogen nuclei (protons) and because its relaxation behavior is well suited for cyclic adiabatic inversion (rotating-frame relaxation time $T_{1\rho} > 1$ s) (*8, 9*). The 100-MHz radio-frequency (rf) field used to excite NMR was generated by a 0.8-mm-diameter coil (2.5 turns) located less than a millimeter from the sample. All measurements were made at room temperature.

The cantilever (Fig. 2) was only 900 Å thick and had a spring constant $k = 1 \times 10^{-3}$ N/m. This spring constant is less than 1/30 of that typically used for atomic force microscopy. When loaded with the sample, the cantilever had a 1.4-kHz mechanical resonance frequency and exhibited an intrinsic quality factor, Q, of 3000 in vacuum. The effective quality factor, Q_{eff}, was typically lower than this value because damping feedback was used to reduce the response time of the cantilever (*10*). The angstrom-scale motion of the cantilever was monitored by a fiber optic interferometer (*11, 12*) and was synchronously detected with a lock-in amplifier.

The root-mean-square (rms) force sensitivity of the apparatus (*13*) was $F_{\min} = 5 \times 10^{-16}$ N, as measured at the cantilever resonance frequency with a lock-in time constant of 1 s [equivalent noise bandwidth $\Delta\nu = 0.25$ Hz (*14*)]. This excellent sensitivity is a direct consequence of the very low spring constant and high intrinsic Q of the cantilever. The sensitivity is limited primarily by the thermal vibration noise of the cantilever. The theoretical sensitivity, assuming thermal noise, is $F_{\min} = (4\,k\,k_B\,T\Delta\nu/Q\omega_c)^{1/2}$, where ω_c is the resonance frequency of the cantilever, k_B is Boltzmann's constant, and T is temperature (*3, 15*). For our cantilever operating at room temperature with a noise bandwidth $\Delta\nu = 0.25$ Hz, the theoretical rms thermal noise level is $F_{\min} = 4 \times 10^{-16}$ N, in good agreement with the experimental value.

The protons in the sample were polarized in the $\hat{z}$ direction by a static field B_z, which was the combination of a homogeneous field (1.95 T) from the superconducting magnet and an inhomogeneous field (~0.4 T) produced by a magnetized iron particle (1.5 mm in diameter, 4 mm long). The iron particle was mounted on a piezoelectric translator and positioned ~700 μm from the sample. The strong magnetic field gradient created by the iron particle ($\partial B_z/\partial z \simeq 600$ T/m) was required to generate a measurable force on the sample and to provide spatial resolution. At thermal equilibrium, the polarizing field produced in the sample a net nuclear magnetic moment given by the Curie law $m_z = NV\mu_p(\mu_p B_z/k_B T)$, where N is the number of protons per unit volume (5.1×10^{22} protons per cubic centimeter), V is the sample volume (7.1×10^{-9} cm^3), and μ_p is the magnetic moment of the proton (1.4×10^{-26} J/T). For our sample, which contained about 3.6×10^{14} protons, the equilibrium magnetic moment in the 2.35-T polarizing field was $m_z = 4.1 \times 10^{-17}$ J/T $= 2.9 \times 10^9\ \mu_p$.

An NMR modulation technique was used to create an oscillating $m_z(t)$ and thereby generate an oscillating magnetic force $F_z(t) = m_z(t)\partial B_z/\partial z$. By choosing the oscillation frequency to be the cantilever resonance frequency, we were able to enhance the resulting cantilever vibration amplitude by the effective Q of the cantilever, thus improving the detectability of the force. An important side benefit of using NMR to create an oscillating force is that it allows nuclear magnetism to be distinguished from other sources of force (for example, electron diamagnetism, van der Waals interactions, and environmental vibrations).

The modulation scheme we adopted was first suggested to us by Sidles (*6*) and is based on cyclic adiabatic inversion (*16*). Under certain conditions, the nuclear magnetic moment viewed in a reference frame rotating at the frequency of the rf excitation can be made to follow the direction of the effective field, $\mathbf{B}_{\text{eff}}$, where

$$\mathbf{B}_{\text{eff}} = B_1\hat{\mathbf{x}} + (B_z - \omega/\gamma)\hat{\mathbf{z}} \qquad (1)$$

Here, B_1 is the amplitude of the applied rf magnetic field, which, in the rotating frame, is a constant field in the $\hat{\mathbf{x}}$ direction, ω is the rf frequency, and γ is the gyromagnetic ratio (2.68×10^8 s^{-1} T^{-1} for protons).

The modulation scheme uses frequency modulation of the rf field to endow $\mathbf{B}_{\text{eff}}$ with an oscillating z component. The rf frequency has the form $\omega(t) = \omega_0 + \Delta\omega(t)$, where ω_0 is the rf carrier frequency and $\Delta\omega(t)$ is the frequency modulation. We now consider the case where the carrier frequency satisfies the resonance condition $\omega_0 = \gamma B_z$, so that $\mathbf{B}_{\text{eff}} = B_1\hat{\mathbf{x}} - (\Delta\omega/\gamma)\hat{\mathbf{z}}$. Starting with no rf excitation, the spins are allowed to polarize in the static field B_z for a time greater than the longitudinal relaxation time T_1 (>4 s) in order to achieve an initial magnetic moment $m_z(0)$. The rf excitation is then set to a frequency below resonance

($\Delta\omega/2\pi \simeq -500$ kHz), and its amplitude is increased slowly (~10 ms). Because of the large frequency offset ($|\Delta\omega/\gamma| >> B_1$), $\mathbf{B}_{\text{eff}}$ remains nearly parallel to the polarizing field. The rf frequency is then swept through resonance and frequency modulated so that $\Delta\omega(t) = \Omega \sin \omega_c t$, where Ω is the peak frequency deviation and ω_c is the cantilever resonance frequency (Fig. 3A). This modulation pattern causes $\mathbf{B}_{\text{eff}}$ to swing toward the x axis and then oscillate below and above the x axis in the xz plane. If the frequency modulation is at a sufficiently slow rate so that the adiabatic condition is satisfied ($|d\mathbf{B}_{\text{eff}}/dt| << \gamma B_1^2$), then the sample moment $\mathbf{m}$ will follow the direction of $\mathbf{B}_{\text{eff}}$ (*17*). When this is the case, $m_z(t)$ is given by

$$m_z(t) = -m_z(0)\,\frac{\Delta\omega(t)/\gamma}{\{[\Delta\omega(t)/\gamma]^2 + B_1^2\}^{1/2}} \tag{2}$$

This oscillating moment (Fig. 3B) creates a cyclic force on the sample and causes the cantilever to vibrate.

Figure 4 shows the cantilever vibration amplitude that developed during a burst of modulation lasting 2.2 s. In response to the oscillating nuclear magnetic moment, the cantilever achieved an rms vibration amplitude of 110 Å, corresponding to an rms magnetic force of 1.1×10^{-14} N. The rms noise level in this single-shot experiment was 5 Å, yielding a signal-to-noise ratio of 22. Because the sample contained 3.6×10^{14} protons, the number of protons corresponding to unity signal-to-noise ratio is 1.6×10^{13}. This sensitivity is close to the theoretically expected value. The minimum detectable magnetic moment is expected to be $m_{\min} = F_{\min}/|\partial B_z/\partial z|$, where $F_{\min}$ is the minimum detectable force. For the experimental conditions in Fig. 4, $F_{\min} = 5 \times 10^{-16}$ N and $\partial B_z/\partial z = 600$ T/m, yielding $m_{\min} = 8.3 \times 10^{-19}$ J/T $= 5.9 \times 10^7\ \mu_p$. Based on the Curie law for protons in a 2.35-T field at 300 K, the number of protons required to generate this rms moment is $n = \sqrt{2}\, m_{\min}/(\mu_p^2 B_z/k_B T) = 1.0 \times 10^{13}$, in good agreement with the experimental value (*18*).

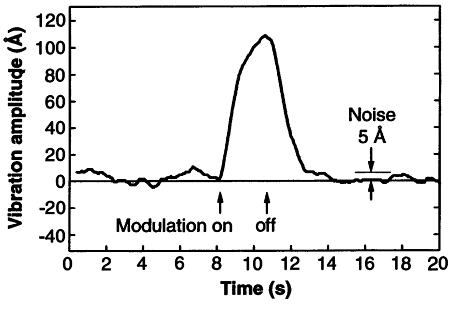

Fig. 4. Time dependence (arbitrary $t = 0$) of the cantilever vibration amplitude measured during a single shot experiment (no averaging) where cyclic adiabatic inversion was started and stopped as indicated. The cantilever achieved an rms amplitude of 110 Å, corresponding to an rms magnetic force of 1.1×10^{-14} N. The 5 Å vibration noise corresponds to a minimum detectable force of $F_{\min} = 5 \times 10^{-16}$ N. The slow rise and fall times of the response are primarily a result of the 1 s time constant of the lock-in amplifier. Measurement conditions: $B_1 = 12$ G, $\Omega/2\pi = 170$ kHz, and $Q_{\text{eff}} = 1000$.

We have verified that the response in Fig. 4 is indeed the result of magnetic resonance by measuring the cantilever vibration amplitude as a function of polarizing field strength and rf frequency. The polarizing field strength at the location of the sample can be controlled by the position of the iron particle. For a given rf frequency, the vibration amplitude reaches a peak when the iron particle is at a specific distance from the sample (Fig. 5). The location of the peak corresponds to the position of the iron particle that generates the resonance field $B_z = \omega_0/\gamma$ at the sample. When the experiment was repeated with the rf frequency increased by $\delta f = 1$ MHz, the iron particle had to be moved closer to the sample by $\delta z = 39$ μm to maintain magnetic resonance. This information can be used to precisely determine the field gradient generated by the iron particle: $|\partial B_z/\partial z| = (2\pi/\gamma)\delta f/\delta z = 6.0 \times 10^2$ T/m. This result is in good agreement with the gradient calculated for the known particle geometry.

Such a large field gradient is desirable for high-resolution NMR imaging. Although some preliminary three-dimensional results have been obtained, we confine the present discussion to one-dimensional imaging in the $\hat{z}$ direction. We have successfully used two different methods. First, we mechanically scanned the iron particle while keeping the rf carrier frequency fixed. This is essentially the same procedure as that used in Fig. 5, where each line scan can be interpreted as a low-resolution spatial map of the spin density projected onto the z axis. The spatial resolution was not optimal in this case because a large modulation amplitude Ω was used.

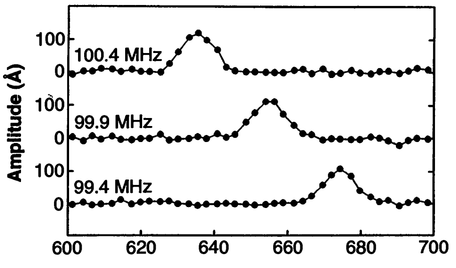

Fig. 5. Cantilever vibration amplitude as a function of the distance from the iron particle to the sample. Each point represents the rms vibration amplitude attained during cyclic adiabatic inversion. The peaks in the data occur when $B_z = \omega_0/\gamma$ at the sample. Higher carrier frequency moves the position of the peak to smaller particle-to-sample spacing, corresponding to higher polarizing field. Measurement conditions: $B_1 = 13.1$ G, $\Omega/2\pi = 108$ kHz, and $Q_{\text{eff}} = 2600$.

In the second method, we fixed the position of the iron particle and scanned the rf carrier frequency, ω_0. As a consequence of the large field gradient, different z positions of the sample experience different values of B_z, corresponding to different NMR resonance frequencies. As ω_0 is scanned, successive slices of the sample go into resonance, each slice generating an oscillating magnetic force in proportion to the number of protons within the slice. A plot of the spin density obtained by this method (Fig. 6) shows that the spin density is confined to a frequency range about 240 kHz wide, corresponding to a sample thickness of 9 μm. The spatial resolution can be estimated from the steepness of the edges of the spin density profile. The right side of Fig. 6 exhibits the steepest response and corresponds to the side of the sample that is adjacent to the flat plane of the cantilever. We estimate the spatial resolution by measuring the width between the 10% and 90% amplitude points. This width, $\Delta f = 67$ kHz, corresponds to a spatial resolution of $\Delta z = 2\pi\Delta f/(\gamma\partial B_z/\partial z) = 2.6$ μm. Theoretically, the expected resolution is approximately $\Delta z = \Delta B/|\partial B_z/\partial z|$, where ΔB is the effective NMR line width. The main contributor to the effective line width is the frequency

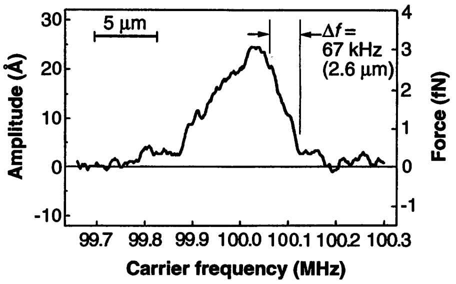

Fig. 6. One-dimensional image of proton density obtained by measuring the cantilever rms vibration amplitude as a function of the rf carrier frequency. The 640-kHz frequency range was scanned in 5 s with the rf excitation continually on and sinusoidally frequency modulated during the scan. The 120 successive scans were averaged together to improve the signal-to-noise ratio. The length of the 5-μm scale bar is based on the 600-T/m field gradient present at the sample. A spatial resolution of 2.6 μm was estimated from the 67-kHz width between 10% and 90% amplitude points on the right edge of the spin density profile. Measurement conditions: $B_1 = 8.3$ G, $\Omega/2\pi = 25$ kHz, and $Q_{\text{eff}} = 800$.

modulation. For the modulation conditions used for Fig. 6, an effective line width of ΔB = 16 G was calculated. Combining this with the known field gradient gives Δz = 2.7 μm, in good agreement with the experimental result. This spatial resolution is roughly an order of magnitude better than that obtained by conventional NMR imaging of nonmetallic solid samples (*19*).

The results presented in this report demonstrate that NMR force detection can achieve remarkable sensitivity and spatial resolution. Further advances are expected as progress is made toward more-sensitive cantilevers, higher field gradients, and lower temperatures. This work is also significant for the field of scanning probe microscopy. Previous scanning probes—including tunneling, atomic force, and near-field optical microscopies—have so far measured only the electronic properties of the sample. Now, we have shown that nuclear magnetism is also accessible.

REFERENCES AND NOTES

1. J. A. Sidles, *Appl. Phys. Lett.* **58**, 2854 (1991).
2. ______, *Phys. Rev. Lett.* **68**, 1124 (1992).
3. ______, J. L. Garbini, G. P. Drobny, *Rev. Sci. Instrum.* **63**, 3881 (1992).
4. D. Rugar, C. S. Yannoni, J. A. Sidles, *Nature* **360**, 563 (1992).
5. O. Züger and D. Rugar, *Appl. Phys. Lett.* **63**, 2496 (1993).
6. J. A. Sidles suggested cyclic adiabatic inversion as a means to create a slowly oscillating nuclear magnetic moment (personal communication).
7. The processing steps for the fabrication of the cantilevers included (i) low-pressure chemical vapor deposition of silicon nitride onto ⟨110⟩-oriented silicon substrates, (ii) patterning of the silicon nitride by photolithography and reactive ion etching, (iii) release of the cantilevers by KOH etching of the underlying silicon substrate, and (iv) critical point drying with high-pressure carbon dioxide. For further details, see S. Hoen *et al.*, in *Technical Digest of the 1994 Solid-State Sensor and Actuator Workshop*, Transducers Research Foundation, Hilton Head, SC, 13 to 19 June 1994 (in press).
8. M. T. Riggin, R. R. Knispel, M. M. Pintar, *J. Chem. Phys.* **56**, 2911 (1972).
9. H.-M. Vieth *et al.*, in preparation.
10. J. Mertz, O. Marti, J. Mlynek, *Appl. Phys. Lett.* **62**, 2344 (1993). In our case, damping feedback was implemented with a piezoelectric element attached to the cantilever holder. Unlike viscous damping, feedback-induced damping does not degrade the signal-to-noise ratio of the force detection.
11. D. Rugar, H. J. Mamin, P. Guethner, *Appl. Phys. Lett.* **55**, 2588 (1989).
12. T. R. Albrecht, P. Grütter, D. Rugar, D. P. E. Smith, *Ultramicroscopy* **42–44**, 1638 (1992).
13. We define the force sensitivity, F_{min}, as the rms amplitude of the sinusoidal force required to produce a dc signal level at the output of the lock-in amplifier equal to the rms noise at the lock-in output.
14. Application note #3 on lock-in amplifier principles, Stanford Research Systems (Sunnyvale, CA).
15. U. Dürig, O. Züger, A. Stalder, *J. Appl. Phys.* **72**, 1778 (1992).
16. A. Abragam, *The Principles of Nuclear Magnetism* (Oxford Univ. Press, London, 1961), pp. 86 and 545–548.
17. C. P. Slichter, *Principles of Magnetic Resonance* (Springer-Verlag, Berlin, 1990), p. 24.
18. The slight discrepancy between the experimental and theoretical results is attributable to the fact that part of the sample is off resonance because of the large field gradient and the finite thickness of the sample.
19. For a review of solid-state NMR imaging, see, for example, D. G. Cory, in *Annual Reports on NMR Spectroscopy*, G. A. Webb, Ed. (Academic Press, London, 1992), vol. 24, pp. 87–180.
20. We thank J. A. Sidles for many enlightening communications and for his suggestion of cyclic adiabatic inversion. We also thank T. Albrecht, P. Grütter, D. P. E. Smith, and H. J. Mamin for their contributions to a previous version of the force detection apparatus. Some of the cantilever fabrication steps were performed at the Microfabrication Laboratory, University of California at Berkeley. The help of G. T. Mulhern with the critical point drying process was especially appreciated. O.Z. gratefully acknowledges financial support by the Swiss National Science Foundation.

27 January 1994; accepted 25 April 1994

Methane to Ethylene with 85 Percent Yield in a Gas Recycle Electrocatalytic Reactor-Separator

Y. Jiang, I. V. Yentekakis, C. G. Vayenas

Methane was oxidatively coupled to ethylene with an ethylene yield up to 85 percent and a total C_2 hydrocarbon yield up to 88 percent in a gas recycle high-temperature (800°C) electrocatalytic or catalytic reactor where the recycled gas passes continuously through a molecular sieve trap in the recycle loop. Oxygen is supplied either electrocatalytically by means of the solid electrolyte support of the silver-based catalyst or in the gas phase. The C_2 products are obtained by subsequent heating of the molecular sieve trap. The selectivity to ethylene is up to 88 percent for methane conversion up to 97 percent.

The oxidative dimerization, or "coupling," of methane to the C_2 hydrocarbons ethane and ethylene with C_2 hydrocarbon yield Y_{C_2} in excess of 50% and ethylene yield $Y_{C_2H_4}$ higher than 40% has been a long-sought goal in heterogeneous catalysis (*1–8*). Achieving these threshold values is considered a necessary requirement for the development of an economically viable industrial process for the one-step production of ethylene from natural gas.

Since the seminal work of Keller and Bhasin (*2*), numerous catalysts have been found (*3–9*) that give selectivity to C_2 hydrocarbons (denoted by S_{C_2}) higher than 90% for low (<2%) methane conversion (hereafter denoted by C_{CH_4}). However, it was universally found (*2–9*) that the total C_2 hydrocarbon selectivity S_{C_2} and ethylene selectivity $S_{C_2H_4}$ decrease drastically with increasing conversion C_{CH_4}, so that Y_{C_2} (which equals $C_{CH_4}S_{C_2}$) and $Y_{C_2H_4}$ (equal to $C_{CH_4}S_{C_2H_4}$)are always less than 30% and 15%, respectively.

In a recent pioneering paper, Aris and co-workers (*10*) showed that Y_{C_2} and $Y_{C_2H_4}$ can be increased up to at least 50% and 17%, respectively, by using a Sm_2O_3 catalyst in a simulated countercurrent moving-bed chromatographic reactor (SCMBCR) to carry out the oxidative coupling of methane (OCM) reaction. In this reactor, the methane-oxygen feed is cycled periodically between four reactor units, maintained at a high (50:1) methane-to-oxygen ratio, and four separating columns; the procedure is repeated indefinitely.

The reason for the low $S_{C_2H_4}$ and S_{C_2} values at high methane conversion C_{CH_4} and thus the reason for the low measured Y_{C_2} and $Y_{C_2H_4}$ values of earlier studies (*2–9*) is that the desired products ethylene and ethane are far more reactive with oxygen than with methane and therefore are easily oxidized to CO or CO_2 when their concentrations become comparable to that of methane (that is, for high methane conversion). Consequently, the observed improvement in C_2 yield (~50%) in the case of the SCMBCR (*10*) is attributable to the partial separation and removal of C_2 hydrocarbons from unreacted methane and oxygen. The same is predicted to apply for the countercurrent moving-bed chromatographic reactor (*10*).

We have almost entirely eliminated the problem of the high reactivity of the C_2 hydrocarbons during the OCM reaction by using a gas recycle reactor with a selective Ag-based OCM catalyst or electrocatalyst combined with an appropriate molecular sieve trap in the recycle loop (Linde molecular sieve 5A maintained at 30°C), which traps and thus protects an easily controllable percentage (up to 100%) of ethylene and of ethane produced during each gas cycle. An important feature of this molecular sieve material is that it traps ethylene much more effectively than ethane and thus leads to very high ethylene yields. In this way, we have obtained C_2 hydrocarbon yield values Y_{C_2} up to 88% and, more importantly, ethylene yield values $Y_{C_2H_4}$ up to 85%.

Department of Chemical Engineering, University of Patras, Patras GR-26500, Greece.